Synthesis of 3-Pol Low-Cost Phased Arrays Via Element Polarization Optimization

Eren Hamamcı[#$], Jonas Heylen[#$], Guilherme Theis[$], Yanki Aslan[#]

[#]Department of Microelectronics, TU Delft, The Netherlands
[$]Robin Radar Systems, The Netherlands
e.hamamci@student.tudelft.nl

***Abstract* — A novel element polarization optimization and phase quantization technique is proposed for the low-cost synthesis of three polarizations from active phased arrays. The horizontally (H) and vertically (V) polarized element ports are optimally combined with a fixed phase shift between them. For algorithm demonstration, pattern constraints for H, V, and an arbitrary third polarization, left-handed circular polarization (LHCP), are embedded in the goal function in a 16 by 16 array. It is demonstrated that including the LHCP in the optimization significantly improves its gain and side lobe levels, compared to when it is not included, at the cost of a slight reduction in the gain of the H/V polarized patterns. The side lobe and cross-polarization levels of H/V polarized patterns remain similar.**

***Keywords* — Array architecture, array synthesis, pattern optimization, polarimetric phased arrays, polarization control.**

I. Introduction

Polarimetric phased arrays attract increased interest in various sensing and communication applications. In weather radars, polarimetry provides information about the size, shape, and orientation of the precipitation particles [1]. Sensing is usually performed by either alternately activating the horizontal (H) and vertical (V) polarizations, or by transmitting both of them simultaneously. The H and V directions correspond to the angular unit vectors in a spherical coordinate grid. However, to retrieve all possible polarimetric information, nine degrees of freedom must be retrieved, which requires transmission of at least three different polarizations [2]. This method is referred to as 3Pol1D in the weather radar literature [3]–[5]. In wireless communications, tri-polarized antennas were proposed as well, with the aim of tripling the capacity [6]. However, this technique has not been widely used due to increased array hardware and processing complexity.

Recently, an element polarization optimization technique was proposed in [7], which reduces the array complexity significantly by combining the H, V ports of each element in a single radio frequency (RF) chain (see Fig. 1). The fixed phase shift (or time delay) at the V-port of an element determines its polarization state. The work in [7] demonstrated that by optimizing the phases at the V-ports, and the digital weights in baseband, two (H and V) polarizations can be generated by the low-cost topology in Fig. 1b, with similar gain, sidelobe and cross-polarization performance of the conventional topology in Fig. 1a. However, the performance drops considerably when a third (e.g. slant, circular) polarization is desired.

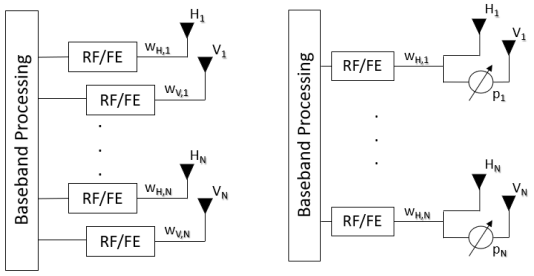

(a) (b)

Fig. 1. Polarimetric phased array architectures: (a) conventional, (b) low-cost with optimally polarized elements (RF/FE: RF front-end, $p_1, ...p_N$ are fixed).

In this paper, we propose an enhanced element polarization optimization algorithm, together with a novel phase quantization technique, to obtain the phase shifts $[p_1, ...p_N]$ for reasonably well array pattern performances for three polarizations (H, V and an arbitrary polarization). Section II formulates the problem and explains the proposed optimization methodologies. Section III provides and discusses the simulation results. Section IV concludes the paper.

II. Formulation of the Optimization Problem

A. Array Pattern Synthesis

For a single-polarized array composed of N radiators, the array far-field pattern in spherical coordinate system angles (ϑ, φ) is given as follows:

$$F(\vartheta,\varphi) = \sum_{i=1}^{N} w_n a_n(\vartheta,\varphi) = \mathbf{a}^H(\vartheta,\varphi)\mathbf{w} \tag{1}$$

where $\mathbf{w}$ and $\mathbf{a}(\vartheta,\varphi)$ represent the vectors containing the beamforming coefficients with maximum amplitude of 1, and complex active element patterns (AEP) of the radiators, respectively. When the fully polarized array in Fig. 1a is considered, the polarimetric (H, V) components of (1) become:

$$F_H(\vartheta,\varphi) = \mathbf{a}_{HH}^H(\vartheta,\varphi)\mathbf{w}_H + \mathbf{a}_{HV}^H(\vartheta,\varphi)\mathbf{w}_V \tag{2}$$

$$F_V(\vartheta,\varphi) = \mathbf{a}_{VV}^H(\vartheta,\varphi)\mathbf{w}_V + \mathbf{a}_{VH}^H(\vartheta,\varphi)\mathbf{w}_H \tag{3}$$

where, for example, $\mathbf{a}_{HV}$ denotes the H field generated by the V port of the antenna. By properly optimizing $\mathbf{w}_H$ and $\mathbf{w}_V$, the desired co-polarization can be synthesized and the orthogonal

cross-polarization can be suppressed. In comparison, for the low-cost architecture in Fig. 1b, (1) becomes:

$$F_H(\vartheta,\varphi) = \mathbf{a}_{HH}^H(\vartheta,\varphi)\mathbf{w}_H + \mathbf{a}_{HV}^H(\vartheta,\varphi)\mathbf{w}_H \odot \mathbf{p} \quad (4)$$

$$F_V(\vartheta,\varphi) = \mathbf{a}_{VV}^H(\vartheta,\varphi)\mathbf{w}_H \odot \mathbf{p} + \mathbf{a}_{VH}^H(\vartheta,\varphi)\mathbf{w}_H \quad (5)$$

where $\mathbf{p} = \begin{bmatrix} p_1 & \cdots & p_N \end{bmatrix}^T$ are the fixed phases at the V-ports of each antenna, and $\odot$ is the Hadamard product.

B. Synthesis of an Arbitrary Third Polarization

By using the Jones transformation matrix, any arbitrary (third) polarization can be expressed through H/V:

$$\begin{bmatrix} F_{co} \\ F_{cr} \end{bmatrix} = \begin{bmatrix} \cos(\phi) & \sin(\phi) \\ -\sin(\phi) & \cos(\phi) \end{bmatrix} \begin{bmatrix} 1 & 0 \\ 0 & e^{-j\eta} \end{bmatrix} \begin{bmatrix} F_H \\ F_V \end{bmatrix} \quad (6)$$

$$F_{co}(\vartheta,\varphi) = \cos(\phi)F_H(\vartheta,\varphi) + \sin(\phi)e^{-j\eta}F_V(\vartheta,\varphi) \quad (7)$$

$$F_{cr}(\vartheta,\varphi) = -\sin(\phi)F_H(\vartheta,\varphi) + \cos(\phi)e^{-j\eta}F_V(\vartheta,\varphi) \quad (8)$$

where ϕ is the orientation angle, and η is the phase difference between the orthogonal fields.

C. Optimization Framework

The flow chart for the optimization procedure is shown in Fig. 2. The antenna elements are assumed to be isotropic radiators and the H/V port coupling is ignored, as in [7] for a direct and fair comparison of the results, which leads to:

$$F_H(\vartheta,\varphi) = \mathbf{a}_{HH}^H(\vartheta,\varphi)\mathbf{w}_H = \mathbf{a}^H(\vartheta,\varphi)\mathbf{w}_H \quad (9)$$

$$F_V(\vartheta,\varphi) = \mathbf{a}_{VV}^H(\vartheta,\varphi)\mathbf{w}_H \odot \mathbf{p} = \mathbf{a}^H(\vartheta,\varphi)\mathbf{w}_H \odot \mathbf{p} \quad (10)$$

The goal function and constraints of the optimization are generated based on the field equations given in (9), (10) and the desired polarization states. As can be seen in (10), unlike the dual-polarized architecture, optimization variables of the low-cost architecture $(\mathbf{w}_H, \mathbf{p})$ are in entry-wise product form, making the problem non-convex. The problem can be put into convex form using the semidefinite relaxation method (SDR) and variables can be jointly optimized [8]. However, joint optimization of the variables will enable the array to work perfectly for a single desired polarization but poorly for other polarizations. Therefore, a sequential approach is preferred [7]. In the first stage, $\mathbf{p}$ is optimized for a constant $\mathbf{w}_H$ input such that the array will result in minimum cross-polarization level for multiple desired polarizations. In the second stage, with respect to the fixed $\mathbf{p}$, $\mathbf{w}_H$ is optimized for any of the intended polarizations of the array. The goal is to make the performance of the low-cost architecture as close as possible to the one of the conventional architecture for three intended polarizations.

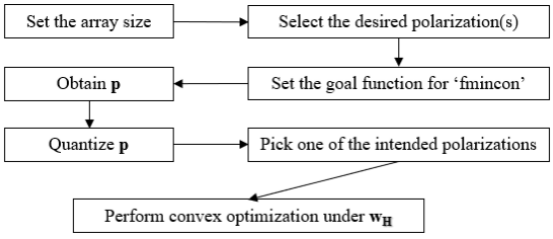

Fig. 2. Flowchart of the overall polarimetric array synthesis procedure.

1) 1st Stage: Element Polarization Optimization

The optimization problem of the first stage is not convex, as $\mathbf{p}$ is a phase shifter and has the form of a complex exponential: $\| p_i \|_2 = ||e^{j\alpha_i}||_2 = 1$, which is not an affine equality constraint. To solve this, the built-in *fmincon* function of Matlab is used [7]. Two novel methods are proposed:

(i) Polarization Averaging (PA):

H-ports are assumed to be uniformly excited, $\mathbf{w}_H$=**1**, and $\mathbf{p}$ is optimized. The architecture is intended to achieve good performance for three different polarization states where two of them are H/V and the remaining one is a linear combination of the two. When $\mathbf{p}$ is optimized with respect to one of H/V, a third polarization can be easily synthesized by properly optimizing $\mathbf{w}_H$ in the second stage. Therefore, the goal function of this stage is based on the cross-polarization levels of one of the H/V and the remaining polarization:

$$\min_{\mathbf{p}} \| \epsilon\mathbf{F}_{cr1}(\vartheta,\varphi), (1-\epsilon)\mathbf{F}_{cr2}(\vartheta,\varphi) \|_\infty \text{ s.t. } \mathbf{w}_H = \mathbf{1} \quad (11)$$

where $\mathbf{F}(\vartheta,\varphi)_{cr1}$ and $\mathbf{F}(\vartheta,\varphi)_{cr2}$ denote the cross polarizations with respect to the two co-polarizations to be optimized. A slack variable ϵ is introduced into the objective function to give importance to any desired polarization. By varying ϵ, cross-polarization levels can be manipulated.

(ii) Common Polarization Suppression (CPS):

This method employs a single cross-polarization to be suppressed over the angular range. As before, H-ports are assumed to be uniformly excited:

$$\min_{\mathbf{p}} \quad \| \mathbf{F}_{cr,mid}(\vartheta,\varphi) \|_\infty \text{ s.t.} \quad \mathbf{w}_H = \mathbf{1} \quad (12)$$

where $\mathbf{F}(\vartheta,\varphi)_{cr,mid}$ denotes the cross-polarization of a state that is in-between the two reference cross-polarizations.

2) 2nd Stage: Digital Beamforming

Once the $\mathbf{p}$ vector is obtained and quantized in the 1st stage, $\mathbf{w}_H$ can be optimized in the 2nd stage by using (7) and (8) with the following goal and constraints:

$$\begin{aligned} \min_{\mathbf{w}_H} \quad & -\mathbb{R}(F_{co}(\vartheta_0,\varphi_0)) = -\rho \\ \text{s.t.} \quad & F_{cr}(\vartheta_i,\varphi_i) \le \rho \cdot 10^{\frac{XPL}{20}}, \quad \forall(\vartheta_i,\varphi_i) \in ML \\ & F_{cr}(\vartheta_i,\varphi_i) \le \rho \cdot 10^{\frac{SLL_{cr}}{20}}, \quad \forall(\vartheta_i,\varphi_i) \in SL \\ & F_{co}(\vartheta_i,\varphi_i) \le \rho \cdot 10^{\frac{SLL_{co}}{20}}, \quad \forall(\vartheta_i,\varphi_i) \in SL \\ & \|\mathbf{w}_{H,i}\|_2 \le 1, \quad \forall i = 1,\cdots,N \end{aligned} \quad (13)$$

where (ϑ_0,φ_0) denotes the main-lobe direction, ML and SL represent the main-lobe and side-lobe angular regions. XPL is the maximum allowed cross-polarization level inside the main-lobe, and SLL_{co} and SLL_{cr} are maximum allowed co- and cross-polarizations inside the side-lobe region in dB. The purpose is to maximize the co-polarization gain in the main-lobe direction; therefore, negative of the gain is minimized instead. However, rather than dealing with the *l2* norm of the gain, its real part is chosen for the objective function [9]. Since the objective function is linear and all

the constraints are convex, the overall optimization problem is convex and existing libraries [10] are used to solve it. It is worth noting that mutual coupling can be included by replacing $\mathbf{a}^H$ with the embedded element responses obtained from full-wave simulations, which is not in the scope of this paper.

D. Phase Quantization

Quantization of the continuous phases optimized in the first stage (assuming two bits as in [7]) is performed with two different methods: (i) regular quantization into one of the levels $(-90°, 0°, 90°, 180°)$ by using a minimum distance function [7], and (ii) using the Lloyd-Max quantization algorithm. Lloyd-Max is an iterative algorithm that searches for the best possible reference phase. The algorithm can be summarized as follows. Initially, equally spaced arbitrary levels and halfway points between them are calculated. Secondly, mean of the continuous phases that are in the same region (defined by the midway points) are found, which become the new quantized levels. The next step is to calculate the new mid-points and the mean of each region. The process continues until there is no significant change in quantized levels. To have a fair comparison with the regular quantization, four levels with $90°$ in between are also considered for the Lloyd-Max algorithm.

III. Simulation Results

A 16 by 16 array where the elements are located half wavelength apart from each other in the two axes is chosen for the simulations [7]. The chosen polarization states are: H ($\phi = 0°, \eta = 0°$), V ($\phi = 90°, \eta = 0°$), and LHCP ($\phi = 45°, \eta = 90°$) as the arbitrary third polarization. A discretized uv-grid ($u = \sin\vartheta\cos\varphi, v = \sin\vartheta\sin\varphi$) is used with a regular step size of 0.05 during the optimization to relax the computational complexity. The co-pol. gain values are computed numerically by taking the ratio of radiation intensity in the scan direction to the average radiated power.

A. Benchmark Techniques

The polarimetric performance of the conventional dual-polarized architecture is shown in Table 1. Convex optimization is utilized to derive the results. The absolute values of gains are shown, while the SLL_{co} is normalized with respect to the maximum gain, which is aimed to be less than -20 dB. The XPL and SLL_{Cr} are not given as the algorithm does not excite the port synthesizing cross-polarization for a predefined co-polarization. It is worth noting that the constraints in (13) are not fully met even with the conventional architecture due to the uv-grid discretization. Improving the grid resolution will improve the SLL results, but this will significantly increase the computational burden.

Furthermore, Table 2 shows the performance of the low-cost architecture with the optimization and phase quantization techniques used in [7]. It can be seen that the gain of the LHCP drop can be greater than 5 dB as compared to the conventional architecture, which clearly motivates our work on 3-pol synthesis with the same low-cost architecture.

Table 1. Polarimetric performance (in dB) of the conventional architecture.

Direction	(ϕ, η)	Gain	SLL_{Co}
Broadside $[u_s = v_s = 0]$	(0,0)	25.3	-18.7
	(90,0)	25.3	-18.7
	(45,90)	25.3	-18.6
Steered $[u_s = v_s = 0.5]$	(0,0)	23.8	-17.7
	(90,0)	23.8	-17.7
	(45,90)	23.7	-17.7

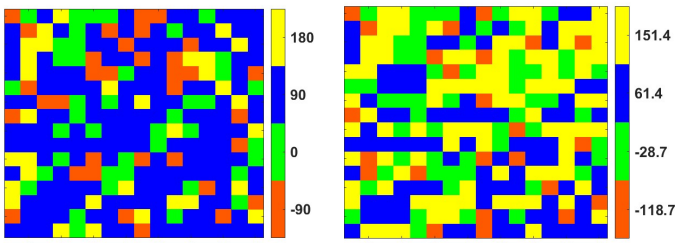

(a) (b)

Fig. 3. Fixed V-port phases optimized in the 1st stage: (a) CPS - Regular Quantization; (b) CPS - Lloyd-Max Quantization.

B. Proposed Element Polarization Optimization Techniques

In PA, cross-polarizations of H and LHCP are put into the objective function given in (11). Through manual tuning ϵ is taken to be 0.6 as it results in a higher H/V gain without a significant loss in LHCP. Although V is not directly inserted into the objective function, array will be able to synthesize it by proper optimization of $\mathbf{w}_H$ if decent performance can be obtained for H. On the other hand, in CPS, the optimization of $\mathbf{p}$ is performed with respect to a single polarization. By direct search, it is found that ($\phi = 27°, \eta = 90°$) yields the best pattern results. The quantized phases with both quantization methods for CPS are also given in Fig. 3a and 3b.

After obtaining the fixed phase shifts in the 1st stage, $\mathbf{w}_H$ is optimized using the convex problem given in (13) with respect to the 3 polarizations, separately for each $\mathbf{p}$ vector in the 2nd stage. Constraints are set as: $XPL = -45$ dB, $SLL_{cr} = SLL_{co} = -20$ dB [7]. Two different scenarios are considered: broadside radiation and steering to $45°$ in both elevation (ϑ) and azimuthal (φ) planes, which is $u_s = v_s = 0.5$ [7].

The radiation performance obtained from the two proposed methods and the two different quantization strategies are shown in Tables 3-4. It is observed that CPS performs better than PA due to more intelligent selection of the common polarization state to be suppressed. Compared to previously published results in [7], the proposed 3-pol synthesis technique (with CPS and regular quantization) significantly increases the gain of the third polarization, LHCP, by approximately 3 dB, while making a large trade-off in the H/V gains (by less than 1.5 dB). Using CPS with Lloyd-Max quantization balances the gains such that the LHCP gain increases by 1.5 dB, while the H/V gains reduce slightly (by less than 0.5 dB), while keeping similar cross-pol. and side lobe performances to the ones obtained by the benchmark techniques. For completeness, several array patterns obtained via the proposed CPS technique with Lloyd-Max quantization are plotted in Fig. 4.

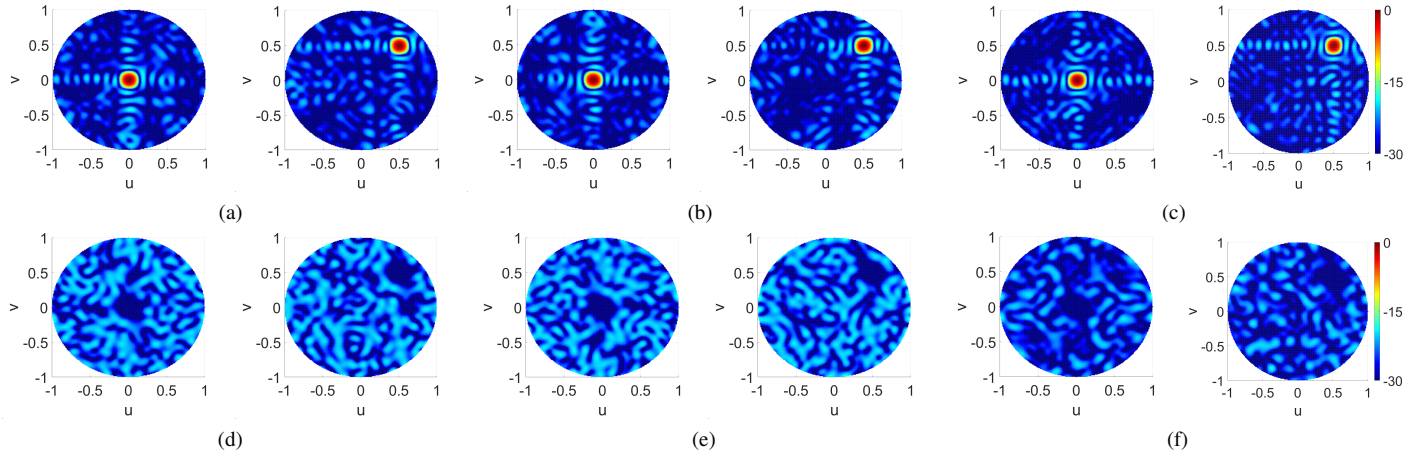

Fig. 4. Array radiation patterns in the uv-plane (normalized, in dB) with the proposed CPS technique with the Lloyd-Max quantization for a broadside $[u_s = v_s = 0]$ and a scanned $[u_s = v_s = 0.5]$ beam: (a) $(\phi = 0°, \eta = 0°)$ - co-pol., (b) $(\phi = 90°, \eta = 0°)$ - co-pol., (c) $(\phi = 45°, \eta = 90°)$ - co-pol., (d) $(\phi = 0°, \eta = 0°)$ - cross-pol., (e) $(\phi = 90°, \eta = 0°)$ - cross-pol., (f) $(\phi = 45°, \eta = 90°)$ - cross-pol.

Table 2. Polarimetric performance (in dB) of the low-cost architecture with the element polarization optimization technique used in [7].

Quant.	Direction	(ϕ, η)	Gain	XPL	SLL_{Co}	SLL_{Cr}
Reg.	Broadside $[u_s = v_s = 0]$	(0,0)	20.8	-43.1	-18.2	-17.3
		(90,0)	20.8	-43.1	-18.2	-17.3
		(45,90)	20.1	-45.2	-18.2	-18.9
	Steered $[u_s = v_s = 0.5]$	(0,0)	20.2	-42.2	-18.2	-16.1
		(90,0)	20.2	-43.0	-18.2	-16.1
		(45,90)	19.4	-42.6	-15.0	-17.7

Table 3. Polarimetric performance (in dB) of the low-cost architecture with the proposed Polarization Averaging (PA) technique.

Quant.	Direction	(ϕ, η)	Gain	XPL	SLL_{Co}	SLL_{Cr}
Reg.	Broadside $[u_s = v_s = 0]$	(0,0)	19.6	-41.8	-14.7	-17.1
		(90,0)	19.6	-41.8	-14.7	-17.1
		(45,90)	22.2	-48.0	-17.9	-23.0
	Steered $[u_s = v_s = 0.5]$	(0,0)	19.1	-41.4	-14.9	-15.0
		(90,0)	19.1	-41.6	-14.8	-15.3
		(45,90)	21.3	-48.8	-17.7	-22.6
Lloyd	Broadside $[u_s = v_s = 0]$	(0,0)	20.3	-42.4	-16.1	-17.5
		(90,0)	20.3	-42.4	-16.1	-17.5
		(45,90)	20.7	-44.0	-17.4	-18.9
	Steered $[u_s = v_s = 0.5]$	(0,0)	19.9	-42.6	-16.7	-18.2
		(90,0)	20.0	-42.9	-16.3	-15.5
		(45,90)	20.4	-43.4	-17.3	-18.8

Table 4. Polarimetric performance (in dB) of the low-cost architecture with the proposed Common Polarization Suppression (CPS) technique.

Quant.	Direction	(ϕ, η)	Gain	XPL	SLL_{Co}	SLL_{Cr}
Reg.	Broadside $[u_s = v_s = 0]$	(0,0)	19.3	-43.3	-18.0	-16.1
		(90,0)	19.3	-43.3	-18.0	-16.1
		(45,90)	23.0	-45.6	-17.0	-21.0
	Steered $[u_s = v_s = 0.5]$	(0,0)	19.1	-43.5	-14.3	-16.4
		(90,0)	19.1	-43.8	-13.7	-15.4
		(45,90)	22.2	-45.2	-17.1	-20.5
Lloyd	Broadside $[u_s = v_s = 0]$	(0,0)	20.2	-43.4	-17.7	-17.8
		(90,0)	20.2	-43.4	-17.7	-17.8
		(45,90)	21.4	-44.6	-18.3	-18.2
	Steered $[u_s = v_s = 0.5]$	(0,0)	19.9	-42.5	-17.1	-17.6
		(90,0)	19.7	-42.9	-16.7	-17.4
		(45,90)	20.7	-42.0	-17.6	-18.6

IV. Conclusion

A novel optimization strategy for a low-cost phased array capable of synthesizing three different polarizations is proposed. Each element has an optimal polarization state, defined by a fixed and quantized phase shift between its H and V ports combined in a single port. Digital beamforming is applied at the element ports. By considering H, V and LHCP patterns in a 16 by 16 array, while incorporating LHCP in the optimization, it is shown that substantial improvements in LHCP gain and side lobe levels are achieved, with minimal trade-off in the performance of the H/V polarizations.

Acknowledgment

This research was supported by the National Growth Fund through the Dutch 6G flagship project “Future Network Services”.

References

[1] A. V. Ryzhkov and D. S. Zrnić, *Radar polarimetry for weather observations*. Springer, 2019, vol. 486.

[2] G. McCormick, “On the completeness of polarization diversity measurements,” *Radio science*, vol. 24, no. 4, pp. 511–518, 1989.

[3] V. Santalla and Y. Antar, “A comparison between different polarimetric measurement schemes,” *IEEE Transactions on Geoscience and Remote Sensing*, vol. 40, no. 5, pp. 1007–1017, 2002.

[4] V. Santalla del Rio, “Least squares estimation of doppler and polarimetric parameters for weather targets,” *IEEE Transactions on Geoscience and Remote Sensing*, vol. 45, no. 11, pp. 3760–3772, 2007.

[5] V. Santalla del Río, J. M. Pidre Mosquera, and M. Vera-Isasa, “3-pol polarimetric weather measurements with agile-beam phased-array radars,” *IEEE Transactions on Geoscience and Remote Sensing*, vol. 52, no. 9, pp. 5783–5789, 2014.

[6] M. R. Andrews, P. P. Mitra, and R. DeCarvalho, “Tripling the capacity of wireless communications using electromagnetic polarization,” *Nature*, vol. 409, no. 6818, pp. 316–318, 2001.

[7] J. Zhou, Z. Wang, Y. Wang, D. Zhu, C. Pang, and Y. Li, “Polarization-reconfigurable phased array architecture with optimally polarized elements,” *IEEE Transactions on Antennas and Propagation*, vol. 73, no. 1, pp. 201–215, 2025.

[8] B. Fuchs, “Application of convex relaxation to array synthesis problems,” *IEEE Transactions on Antennas and Propagation*, vol. 62, no. 2, pp. 634–640, 2014.

[9] B. Fuchs and J. J. Fuchs, “Optimal narrow beam low sidelobe synthesis for arbitrary arrays,” *IEEE Transactions on Antennas and Propagation*, vol. 58, no. 6, pp. 2130–2135, 2010.

[10] I. CVX Research, *CVX: Matlab software for disciplined convex programming, version 2.0*, https://cvxr.com/cvx, Aug. 2012.